Rabi oscillations in a room-temperature quantum dash semiconductor optical amplifier

Amir Capua,[1,*,†] Ouri Karni,[1] Gadi Eisenstein,[1] and Johann Peter Reithmaier[2]

[1]*Electrical Engineering Department, Technion, 32000 Haifa, Israel*

[2]*Institute of Nanostructure Technologies and Analytics, Technische Physik, CINSaT, University of Kassel, 34132 Kassel, Germany*

We report on a direct observation of coherent light-matter interactions imprinted on a short pulse propagating along a room-temperature, electrically biased, quantum dash semiconductor optical amplifier. The principle of the observation is that we characterize the complex field (phase and amplitude) of the short optical pulse after the interaction. By comparing the measurements to a numerical simulation, we are able to decipher the time evolution of effective two-state Schrödinger wave functions representing the ensembles of electronic states along the propagation path. The imprinted signatures on the pulse phase and amplitude stem from the accumulated propagation and reveal systematically clear Rabi oscillations and self-induced transparency. The high sensitivity to the effective ensemble states is shown to result from the response of the refractive index.

PACS number(s): 42.50.Ct, 03.65.−w, 42.55.Px

Observing quantum coherent light-matter interaction requires that the wave function does not dephase during the interaction. Semiconductors, being densely packed interacting atomic systems, exhibit very short dephasing times, which pose a severe limitation to measuring their quantum behavior. This is why the great majority of coherent light-matter interactions in semiconductors were observed in cryogenically cooled systems starting from the paper by Cundiff *et al.* [1]. Taking the form of Rabi oscillations and self-induced transparency [2,3], coherent phenomena in semiconductors were revealed in various structures and materials, including GaAs quantum dots and thin InP layers [4–9], and sensed using different techniques, such as ultrafast spectroscopy [4,10,11], measurements of photogenerated currents [12–14], and precessional motion of spins [15]. The first demonstration of coherent Rabi oscillations observed upon short pulse propagation in an active waveguide was reported only recently [16]. That experiment employed a quantum cascade laser-amplifier device where modifications of the pulse shape were examined by a cross-correlation optical sampling technique.

Observing coherent phenomena in room-temperature solids has also been reported [17,18]; however, in semiconductors, such reports have been scarce. The many-body interactions in semiconductors shorten dramatically the coherence time to values that at room temperature are typically shorter than 500 fs [19,20], thereby obscuring the signatures of the quantum interaction. A remarkable observation of Rabi oscillations occurring in thin, room-temperature GaAs films with a Rabi cycle comparable to the energetic band gap was reported by Mücke *et al.* [21].

In this paper, we present a direct observation of the coherent light-matter interactions, which are built up during the propagation in an electrically driven semiconductor optical amplifier (SOA) operating in room temperature. More importantly, we show that from characterizing the emitted electromagnetic field (phase and amplitude) of the short pulse, the quantum coherent light-matter interaction can be observed and resolved even in the presence of significant room-temperature many-body scattering processes. By a comparison to a numerical simulation of the Maxwell and Schrödinger equations describing the coevolution of the electromagnetic field and a sequence of two-state Schrödinger wave functions, we further show that it is possible to reconstruct the time evolution of an effective two-level system representing the ensembles of quantum states along the waveguide. Depending on the mode of operation (gain or absorption), we demonstrate systematically that the interaction takes on the form of clear, coherent Rabi flopping and self-induced transparency. The pulse chirp turns out to be highly sensitive to the effective state of the ensemble stemming from the dependence of the refractive index on the excited states.

The observations presented here are valid for other semiconductor media of different dimensionalities. Following the results of the present paper [22], Rabi oscillations were also measured in zero-dimensional quantum systems. This was reported in a InP-based quantum dot SOA operating at 1550 nm [23] and in a GaAs-based quantum dot amplifier operating at 1300 nm [24], both exhibiting different state densities and dipole moments compared to the quantum dashes.

The experiment we describe utilized 200-fs-wide pulses, which were used for the excitation and were characterized at the output using a cross-frequency-resolved optical-gating (X-FROG) [25] system with a temporal resolution of a few femtoseconds. The system, which is described schematically in Fig. 1, uses a replica of the input pulse (separately characterized by standard FROG) to gate the output pulse using sum-frequency generation in a nonlinear crystal. The product is measured by a spectrometer as the delay is scanned generating a spectrogram from which the complex envelope of the output pulse is retrieved by a computerized algorithm [25].

The gain section of the 1.5-mm-long SOA is composed of six InAs/InP nanostructured wirelike layers, which are commonly referred to as a quantum dash and were grown by molecular beam epitaxy [26]. A scanning electron microscope image of the wirelike nanostructures [27] is shown in the lower left of Fig. 1. The area coverage is large, ∼30%, with a typical dash that has a base cross-section of 15–20 nm, a height of 3–4 nm, and a length of more than 500 nm. A typical

---

*Corresponding author: acapua@us.ibm.com

†Present address: IBM Research Division, Almaden Research Center, 650 Harry Rd., San Jose, California 95120, USA.
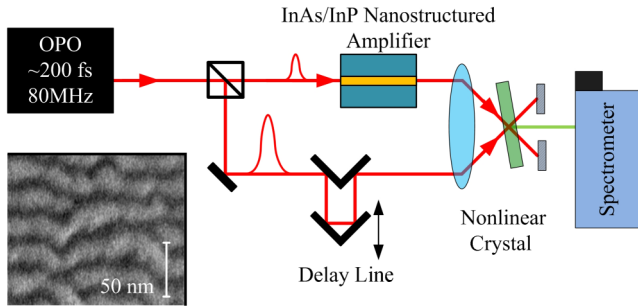
FIG. 1. (Color online) Experimental apparatus. The lower left shows a scanning electron microscope image of the wirelike nanostructured gain medium. OPO, optical parametric oscillator.

inhomogeneously broadened gain spectrum with a width of more than 100 nm at the 10% level below the gain peak is presented in Fig. 2.

The electromagnetic field emitted after the interaction was calculated by solving the Maxwell and Schrödinger equations describing a sequence of two-state Schrödinger's wave functions placed along the propagation axis [16] and fed from a common carrier reservoir. Details of the model are described in Ref. [28].

The calculated propagation of a moderately intense pulse is presented in Fig. 3(a) using the notations of the density matrix formalism. The spatially dependent occupation probability amplitudes in the upper and lower levels of the ground state (marked in the inset as the energy levels E_1 and E_2) ρ_{11} and ρ_{22}, respectively, are plotted along a 60-μm section at a particular time instance. Also shown is the envelope of the pulse Poynting vector in the direction of propagation. As part of the calculation, the fast oscillating coherence terms of the wave function, ρ_{12} and ρ_{21}, were evaluated along the propagation axis as well (not presented). The electronic decoherence time (often referred to as T_2 or γ_{12}^{-1}) used in the calculation was 300 fs. Immediately behind the pulse, the medium is transparent ($\rho_{11} = \rho_{22}$), while it exhibits population inversion ($\rho_{11} > \rho_{22}$) wherever the pulse has not arrived yet. This saturation effect can also be described as a coherent
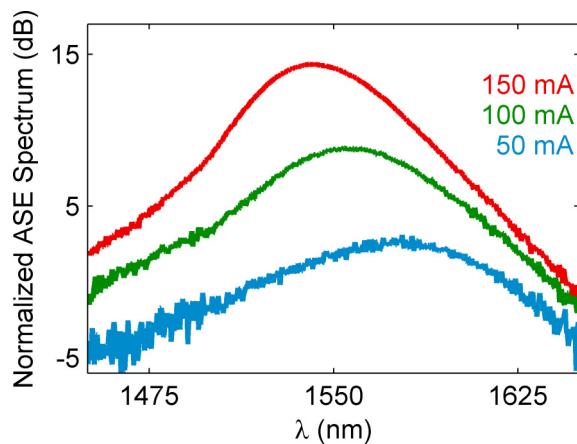

FIG. 2. (Color online) Bias-dependent amplified spontaneous emission (ASE) spectrum of the quantum dash gain medium (normalized).

phenomenon where the transition from gain to transparency is induced by a pulse whose area is $\pi/2$. The low Rabi frequency, $\Omega = \mu E/\hbar$, of this moderate intensity pulse yields a Rabi-oscillation period that is longer than the pulse duration; hence, ρ_{11} and ρ_{22} evolve monotonically during the pulse and exhibit no oscillatory features.

The calculated output pulse intensity profile and instantaneous frequency shift relative to its carrier frequency (pulse chirp) are shown in Fig. 3(b), together with those of the input pulse. Since saturation is moderate, the pulse profile experiences no significant distortion. The behavior of the instantaneous frequency is determined by changes in the refractive index and are inversely proportional to changes in the excited carrier density according to [29]:

$$n^2 = \varepsilon_{r_0} - \varepsilon\left(N_{\mathrm{res}}, \rho_{11}\right) = \varepsilon_{r_0} - C_{\mathrm{res}} N_{\mathrm{res}} - C_{\mathrm{2lev}} \rho_{11} \qquad (1)$$

where ε_{r_0} is the background index and N_{res} is the reservoir carrier density. C_{res} and C_{2lev} describe the index dependence on the reservoir and on the two-level system populations.

Since the carrier density varies during the pulse, this process acts as a phase-sensitive mechanism that imprints the ensemble state on the phase of the electromagnetic field and is a highly detailed description of self-phase modulation taking place along the SOA. An experimental characterization of a $\pi/2$ pulse after traversing the SOA, presented in Fig. 3(c), confirms the calculated predictions.

Increasing the pulse area and correspondingly the Rabi frequency leads to Rabi-oscillation periods, which are shorter than the duration of the pulse. This causes a modulation of the occupation probabilities commonly known as Rabi flopping. A simulation of this process for pulses with an area of 4.4π is shown in Fig. 4(a). Here, the conditions sensed by different parts of the pulse alternate between gain ($\rho_{11} > \rho_{22}$) and coherent absorption ($\rho_{11} < \rho_{22}$). At spatial locations far behind and ahead of the pulse, the conditions are the same as in the classical gain saturation case [Fig. 3(a)]: transparency and population inversion, respectively. The resultant intensity profile at the output exhibits a double peaked pulse, as seen in Fig. 4(b), and the corresponding time-dependent instantaneous frequency, shown also in Fig. 4(b), comprises two valleys that signify two distinct amplification events occurring within the duration of the pulse. The calculated characteristics of this intense, 4.4π pulse were confirmed by X-FROG measurements as described in Fig. 4(c).

Figures 4(b) and 4(c) fit qualitatively well, but they show a difference in the output pulse width. At large pulse areas, the pulse experiences significant two-photon absorption, which broadens the pulses. Two-photon absorption is not included in the model—hence the discrepancy in pulse width. Nevertheless, the main oscillatory behavior in both the intensity profiles and the time-dependent instantaneous frequency traces shown in Fig. 4 testify clearly to the occurrence of distinct Rabi oscillations. Even the slight feature appearing at $t \sim 250$ fs in the calculated instantaneous frequency is observed in the experiment at $t \sim 500$ fs [circled in Figs. 4(b) and 4(c)]. This feature stems from the integrated cumulative effect of the propagating wave and the Rabi-oscillation wave, which builds up along the length of the amplifier. The ability to measure and predict these features means that in the Bloch sphere
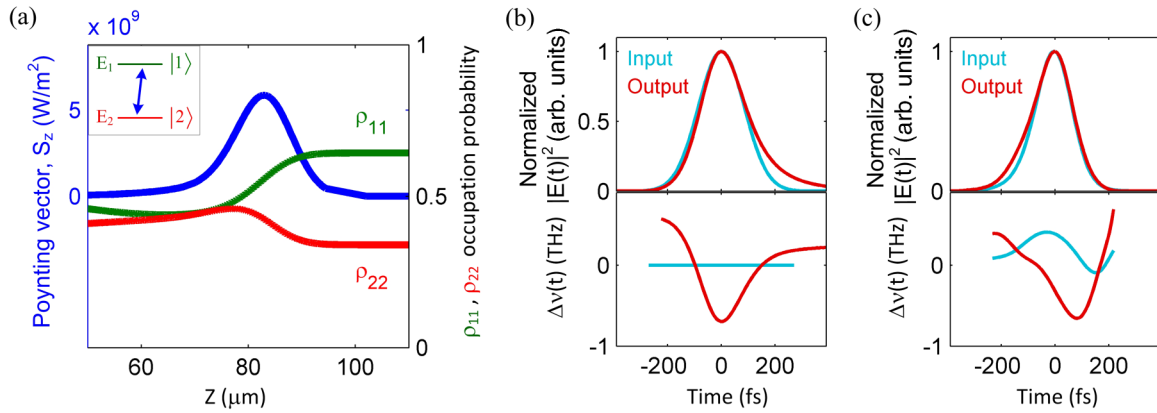
FIG. 3. (Color online) Propagation in the gain regime of a 200 fs pulse whose area is $\pi/2$, causing classical saturation. (a) Simulated spatial distribution of ρ_{11} and ρ_{22}. Shown in blue is the envelope of the pulse Poynting vector along the direction of propagation, S_z. (b) Simulated normalized pulse intensity $|E(t)|^2$ and instantaneous frequency shift $\Delta\nu(t)$ at the input and output of the laser amplifier. (c) Measured normalized pulse intensity and instantaneous frequency shift at the input and output.

description, the trajectory by which the ensemble states evolve can be reconstructed.

The transition from classical saturation to a regime where Rabi oscillations dominate was further investigated by gradually increasing the pulse area, controlling either the input pulse energy or the bias. The dependence on input pulse energy is shown in Fig. 5. The figure shows the simulated [Figs. 5(a) and 5(b)] and measured [Figs. 5(c) and 5(d)] results, with the difference between consecutive traces corresponding to a doubling of the pulse energy ($\sqrt{2}$ multiples of the pulse area). The single-peaked low power pulse profile evolves gradually into a double-peaked shape observed for input pulse areas larger than 2.5π. The time-dependent instantaneous frequency evolves correspondingly from the conventional single-valley shape at low pulse energies to the double-valley functional form representing the two distinct gain events. The first valley, which denotes gain saturation, marks the start of the coherent interaction and shifts to earlier times as the pulse area is increased since saturation occurs earlier for the more intense pulses, which cause shorter Rabi periods. The functional forms of the simulated and the experimental profiles are consistent with each other. Even slight features in the instantaneous frequency traces, for example, two breaks in the 1.7π pulse

case that evolve into two peaks when the pulse energy is doubled (the 2.5π case), are predicted and measured.

An alternative way to increase the pulse area is to operate with larger gain levels while keeping the input pulse energy constant. Figure 6 shows bias-dependent responses for an input pulse whose area is 3.2π. A double-peaked intensity and an instantaneous frequency profile with two valleys are seen, indicating that Rabi oscillations took place. As the bias increases, these two signatures of the coherent interaction become more pronounced; the second peak emerges gradually, while the second oscillation in the instantaneous frequency becomes clearer. In particular, under a large bias, the oscillation lasts for a longer part of the pulse duration, as evident from the second cycle in the instantaneous frequency traces. Once more, the simulation predicts (qualitatively) all details measured by the X-FROG system.

The gain medium is in reality inhomogeneously broadened [26,27] and therefore excites spectral regions with different detunings from resonance, which suggests that a continuum of Rabi frequencies should be initiated simultaneously and may interfere and extinguish the imprints. However, a quantitative evaluation of these other Rabi frequencies shows that they are rather similar to the zero-detuning Rabi frequency.
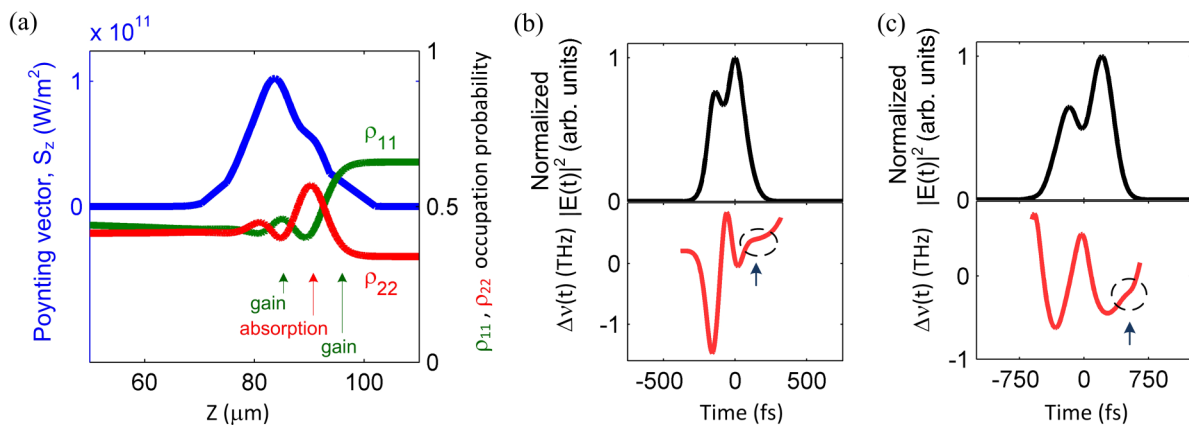

FIG. 4. (Color online) Propagation in the gain regime of an intense $\sim$200 fs pulse whose area is 4.4π. (a) Simulated spatial distribution of ρ_{11} and ρ_{22}. (b) Simulated output pulse amplitude and instantaneous frequency profiles (c) Measured output pulse.
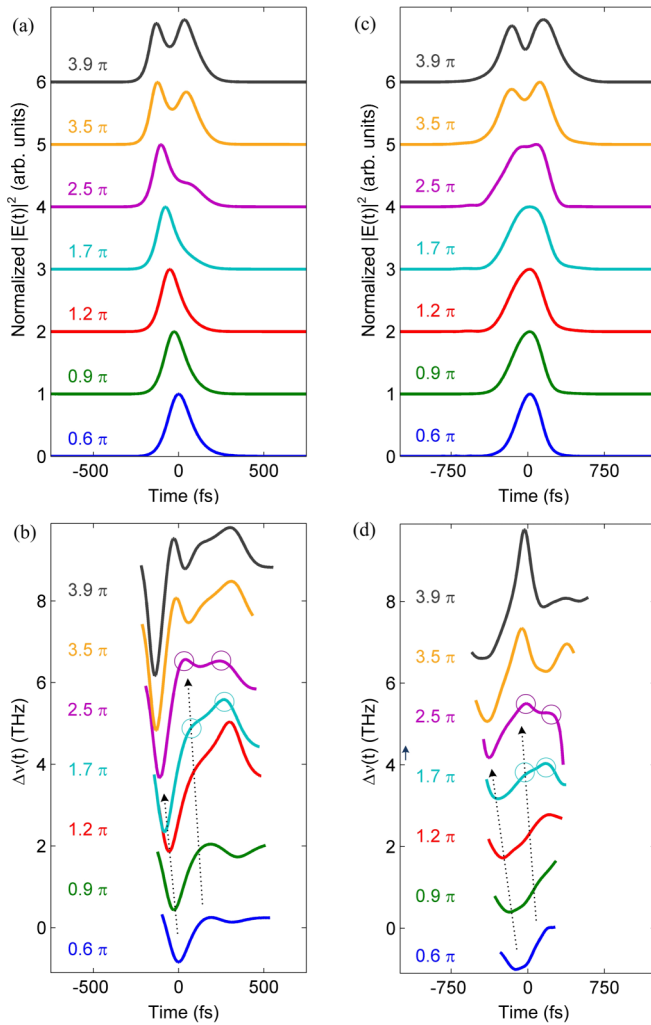
FIG. 5. (Color online) Pulse area dependence of the output pulses. (a) and (b) Simulated normalized output intensity profiles and time-dependent instantaneous frequencies. (c) and (d) Measured normalized output intensity profiles and time-dependent instantaneous frequencies.

FIG. 6. (Color online) Bias dependence of the output pulses. The input pulse area was 3.2π. (a) and (b) Simulated results. (c) and (d) Measured results.

The short pulse duration allows for two Rabi-oscillation periods at most (a 4.4π pulse); therefore, the medium appears to behave as if it oscillates homogeneously with a single common Rabi frequency. This reasoning justifies the effective two-level approximation [16].

The complementary effect to the Rabi oscillations is self-induced transparency [2,3,30]. In this case, the effective two-level system is prepared, prior to the arrival of the electromagnetic field, in its lower state by applying zero bias. Self-induced transparency means that an intense pulse may coevolve with the medium pumping it beyond the transparency point into the gain regime. This requires once more that the period of the Rabi cycle be shorter than the pulse width. As illustrated in the calculated spatial distribution of ρ_{11} and ρ_{22} [Fig. 7(a)], the leading edge of the pulse is absorbed, the following central part undergoes amplification, and the trailing edge is absorbed. Pulse propagation of this kind is well known to result in pulse compression. Actually, Fig. 7(a) shows that an additional gain event is initiated in the trailing part of the pulse.
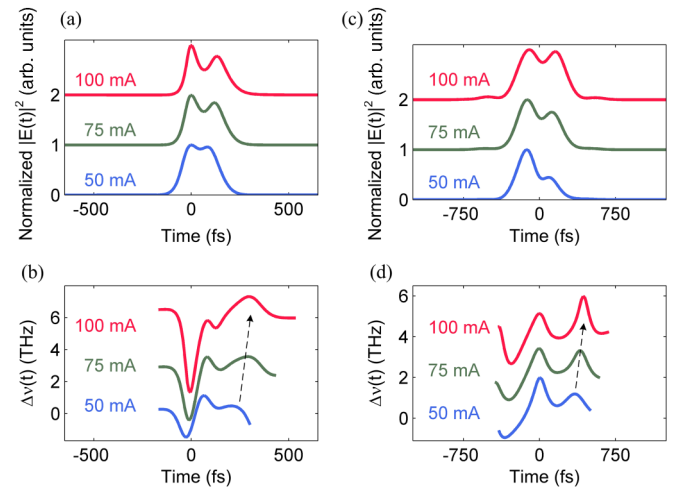
In the zero bias case, the free carrier density is low and its contribution to the refractive index changes is negligible compared to that in the gain regime. Simulating this case therefore requires modifying the refractive index dependence on carrier density given by Eq. (1). The dependence of the refractive index on carrier density was studied thoroughly, theoretically and experimentally, by Zilkie *et al.* [31]. At zero bias, two-photon absorption and stimulated transition heating govern the refractive index dynamics. The combined effects manifest themselves in an opposite index dependence on carrier density [change of sign of C_{res} and C_{2lev} in Eq. (1)] compared to the gain regime.

The intensity profile of Fig. 7(b) shows the expected pulse compression, together with the time-resolved instantaneous frequency. The corresponding X-FROG measurements are presented in Fig. 7(c). While the simulation shows symmetric pulse compression, the experiment shows a clear compression on the trailing edge and a slight compression on the leading edge. In addition, a second trailing excitation in the intensity profile is observed, which also appears in the simulations and indicates that a second oscillation cycle was initiated. The measured time-resolved instantaneous frequency [Fig. 7(c)] is consistent with the simulated result exhibiting a red shift during the pulse peak, which is followed by a sharp frequency increase during the trailing edge. In the absorption regime, the agreement in the pulse duration between the experiment and the calculation is vastly improved compared to the gain regime. This is due to the significantly smaller role that two-photon absorption plays when the direct-gap resonant absorption is present as well.

In conclusion, we have shown that from the measurement of the complex field of a short pulse propagating along the SOA, it is possible to observe the quantum coherent interaction. This is true also in the presence of significant dephasing at room temperatures. The signatures imprinted on the pulse itself resulted from an accumulated propagative effect and enabled us to reconstruct, in the Bloch sphere description, the trajectory by which the effective ensemble states evolved.
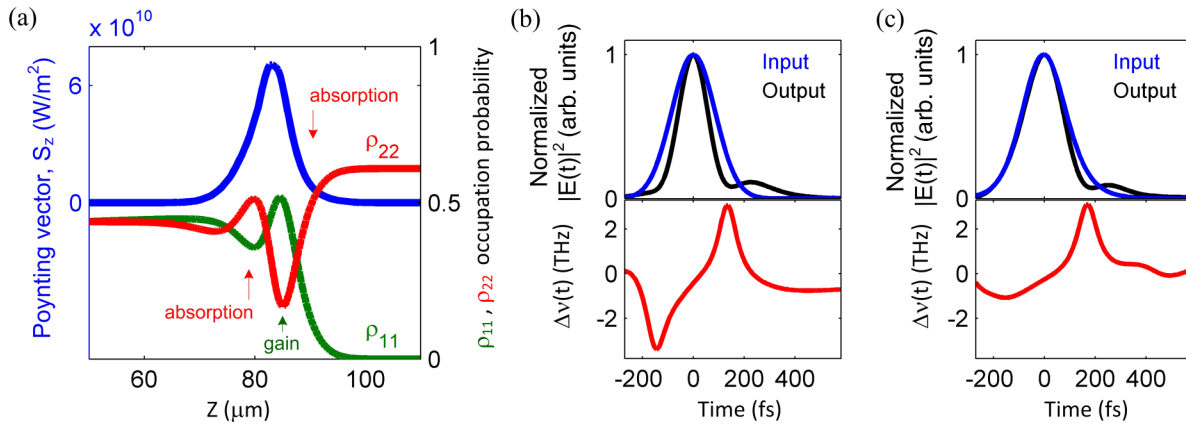
FIG. 7. (Color online) Self-induced transparency. (a) Simulated spatial distribution of ρ_{11} and ρ_{22} for a 3.6π pulse. (b) Simulated normalized output intensity and time-dependent instantaneous frequency. (c) Measured normalized output intensity and time-dependent instantaneous frequency.

Realizing that Rabi oscillations take place along an SOA even at room temperatures, for instance, we can explain now the reason for the sudden increase often observed in the responses of pump-probe experiments at $t = 0$ [32]. In addition, the observations of self-induced transparency, together with nonlinear absorption effects, present directly the mechanisms and limitations that govern passive mode locking in semiconductor lasers.

[1] S. T. Cundiff, A. Knorr, J. Feldmann, S. W. Koch, E. O. Göbel, and H. Nickel, Phys. Rev. Lett. **73**, 1178 (1994).

[2] H. Giessen, A. Knorr, S. Haas, S. W. Koch, S. Linden, J. Kuhl, M. Hetterich, M. Grün, and C. Klingshirn, Phys. Rev. Lett. **81**, 4260 (1998).

[3] M. Jütte and W. von der Osten, J. Lumin. **83-84**, 77 (1999).

[4] C. Fürst, A. Leitenstorfer, A. Nutsch, G. Tränkle, and A. Zrenner, Phys. Stat. Sol. B **204**, 20 (1997).

[5] Y. Wu, I. M. Piper, M. Ediger, P. Brereton, E. R. Schmidgall, P. R. Eastham, M. Hugues, M. Hopkinson, and R. T. Phillips, Phys. Rev. Lett. **106**, 067401 (2011).

[6] H. Htoon, T. Takagahara, D. Kulik, O. Baklenov, A. L. Holmes, Jr., and C. K. Shih, Phys. Rev. Lett. **88**, 087401 (2002).

[7] T. H. Stievater, X. Li, D. G. Steel, D. Gammon, D. S. Katzer, D. Park, C. Piermarocchi, and L. J. Sham, Phys. Rev. Lett. **87**, 133603 (2001).

[8] P. Borri, W. Langbein, S. Schneider, U. Woggon, R. L. Sellin, D. Ouyang, and D. Bimberg, Phys. Rev. B **66**, 081306(R) (2002).

[9] E. B. Flagg, A. Muller, J. W. Robertson, S. Founta, D. G. Deppe, M. Xiao, W. Ma, G. J. Salamo, and C. K. Shih, Nat. Phys. **5**, 203 (2009).

[10] A. Schülzgen, R. Binder, M. E. Donovan, M. Lindberg, K. Wundke, H. M. Gibbs, G. Khitrova, and N. Peyghambarian, Phys. Rev. Lett. **82**, 2346 (1999).

[11] M. U. Wehner, M. H. Ulm, D. S. Chemla, and M. Wegener, Phys. Rev. Lett. **80**, 1992 (1998).

[12] A. Zrenner, E. Beham, S. Stufler, F. Findeis, M. Bichler, and G. Abstreiter, Nature **418**, 612 (2002).

[13] M. Zecherle, C. Ruppert, E. C. Clark, G. Abstreiter, J. J. Finley, and M. Betz, Phys. Rev. B **82**, 125314 (2010).

[14] B. E. Cole, J. B. Williams, B. T. King, M. S. Sherwin, and C. R. Stanley, Nature **410**, 60 (2001).

[15] A. Greilich, R. Oulton, E. A. Zhukov, I. A. Yugova, D. R. Yakovlev, M. Bayer, A. Shabaev, A. L. Efros, I. A. Merkulov, V. Stavarache, D. Reuter, and A. Wieck, Phys. Rev. Lett. **96**, 227401 (2006).

[16] H. Choi, V. M. Gkortsas, L. Dieh, D. Bour, S. Corzine, J. Zhu, G. Höfler, F. Capasso, F. X. Kärtner, and T. B. Norris, Nat. Photon. **4**, 706 (2010).

[17] T. Schwartz, J. A. Hutchison, C. Genet, and T. W. Ebbesen, Phys. Rev. Lett. **106**, 196405 (2011).

[18] T. Gaebel, M. Domhan, I. Popa, C. Wittmann, P. Neumann, F. Jelezko, J. R. Rabeau, N. Stavrias, A. D. Greentree, S. Prawer, J. Meijer, J. Twamley, P. R. Hemmer, and J. Wrachtrup, Nat. Phys. **2**, 408 (2006).

[19] M. Bayer and A. Forchel, Phys. Rev. B **65**, 041308(R) (2002).

[20] J. A. Davis, L. V. Dao, X. Wen, P. Hannaford, V. A. Coleman, H. H. Tan, C. Jagadish, K. Koike, S. Sasa, M. Inoue, and M. Yano, Appl. Phys. Lett. **89**, 182109 (2006).

[21] O. D. Mücke, T. Tritschler, M. Wegener, U. Morgner, and F. X. Kärtner, Phys. Rev. Lett. **87**, 057401 (2001).

[22] A. Capua, O. Karni, G. Eisenstein, and J. P. Reithmaier, arXiv:1210.6803 (2012).

[23] O. Karni, A. Capua, G. Eisenstein, V. Sichkovskyi, V. Ivanov, and J. P. Reithmaier, Optic. Express **21**, 26786 (2013).

[24] M. Kolarczik, N. Owschimikow, J. Korn, B. Lingnau, Y. Kaptan, D. Bimberg, E. Scholl, K. Ludge, and U. Woggon, Nat. Comm. **4**, 2953 (2013).

[25] R. Trebino, *Frequency-Resolved Optical Gating: The Measurement of Ultrashort Laser Pulses* (Kluwer Academic Publishers, Norwell, MA, 2002).

[26] J. P. Reithmaier, G. Eisenstein, and A. Forchel, IEEE Proceedings **95**, 1779 (2007).

[27] H. Dery and G. Eisenstein, IEEE J. Quantum Electron. **40**, 1398 (2004).

[28] A. Capua, O. Karni, and G. Eisenstein, IEEE J. Select. Topic. Quantum Electron. **19**, 1900410 (2013).

[29] T. L. Koch and J. E. Bowers, Electron. Lett. **20**, 1038 (1984).

[30] S. L. McCall and E. L. Hahn, Phys. Rev. **183**, 457 (1969).

[31] A. J. Zilkie, J. Meier, M. Mojahedi, A. S. Helmy, P. J. Poole, P. Barrios, D. Poitras, T. J. Rotter, Y. Chi, A. Stintz, K. J. Malloy, P. W. E. Smith, and J. S. Aitchison, J. Lightwave Technol. **26**, 1498 (2008).

[32] K. L. Hall, G. Lenz, E. P. Ippen, and G. Raybon, Optic Lett. **17**, 874 (1992).